



Hummingbird flight stability and control in freestream turbulent winds.

Citation

Ravi, Sridhar, James D. Crall, Lucas McNeilly, Susan F. Gagliardi, Andrew A. Biewener, Stacey A. Combes. 2015. Hummingbird flight stability and control in freestream turbulent winds. *The Journal of Experimental Biology* 218: 1444-1452.

Published Version

doi:10.1242/jeb.114553

Permanent link

<http://nrs.harvard.edu/urn-3:HUL.InstRepos:14422004>

Terms of Use

This article was downloaded from Harvard University's DASH repository, and is made available under the terms and conditions applicable to Open Access Policy Articles, as set forth at <http://nrs.harvard.edu/urn-3:HUL.InstRepos:dash.current.terms-of-use#OAP>

Share Your Story

The Harvard community has made this article openly available.
Please share how this access benefits you. [Submit a story](#).

[Accessibility](#)

Hummingbird flight stability and control in freestream turbulent winds

Sridhar Ravi^{12*}, James D. Crall¹, Lucas McNeilly, Susan F. Gagliardi¹, Andrew A. Biewener¹ and Stacey A. Combes¹

²Dept. of Organismic and Evolutionary Biology, Harvard University, Cambridge, MA 02138, USA

Present address: ²Sch. Of Aerospace, Mechanical and Manufacturing Engineering, RMIT University, Melbourne, Vic 3000, Australia

* Author for correspondence (Sridhar.ravi@rmit.edu.au)

Abstract

Airflow conditions close to the Earth's surface are often complex, posing challenges to flight stability and control for volant taxa. Relatively little is known about how well flying animals can contend with complex, adverse air flows, or about the flight-control mechanisms employed by animals to mitigate wind disturbances. Several recent studies have examined flight in the unsteady von Kármán vortex streets that form behind cylinders, generating flow disturbances that are predictable in space and time; these structures are relatively rare in nature, as they occur only in the immediate, downstream vicinity of an object. In contrast, freestream turbulence is characterized by rapid, unpredictable flow disturbances across a wide range of spatial and temporal scales, and is nearly ubiquitous in natural habitats. Hummingbirds are ideal organisms for studying the influence of freestream turbulence on flight, as they forage in a variety of aerial conditions and are powerful flyers. We filmed ruby-throated hummingbirds (*A. colubris*) maintaining position at a feeder in laminar and strongly turbulent (intensity ~15%) airflow environments within a wind tunnel, and compared their mean head, body, tail and wing kinematics, as well as variability in these parameters. Hummingbirds exhibited remarkably stable head position and orientation in both smooth and turbulent flow while maintaining position at the feeder. However, the hummingbird's body was less stable in turbulent flow and appeared to be most sensitive to disturbances along the mediolateral axis, displaying large lateral accelerations, translations, and rolling motions during flight. The hummingbirds mitigated these disturbances by increasing mean wing stroke amplitude and stroke plane angle, and by varying these parameters asymmetrically between the wings, and from one stroke to the next. They also actively varied the orientation and fan angle of the tail, maintaining a larger mean fan angle when flying in turbulent flow; this may improve their passive stability, but likely incurs an energetic cost due to increased drag. Overall, we observed many of the same kinematic changes noted previously for hummingbirds flying in a von Kármán vortex street, but we also observed kinematic changes associated with high force production, similar to those seen during load-lifting or high-speed flight. These findings suggest that flight may be particularly costly in fully mixed, freestream turbulence, the flow condition that hummingbirds are likely to encounter most frequently in natural habitats.

Introduction

The Earth's surface directly influences wind profiles within the lowest region of the atmosphere, the Atmospheric Boundary Layer (ABL). Mean and instantaneous properties of wind within the ABL depend upon a number of variables, including large-scale meteorological conditions, solar heating (convective and radiative), and the profile of local terrain (Stull, 1988). The Earth's surface is seldom flat, but rather heterogeneous at multiple size scales, due to both natural (hills, vegetation, etc.) and manmade (buildings, poles, etc.) features. These features act as obstacles to steady air flow, and aerodynamic interactions between the wind and such obstacles lead to unsteady, turbulent flow (Stull, 1988).

Freestream turbulence within the ABL has generally been characterized in terms of its intensity and integral length scale. Turbulence Intensity (Ti), defined as the ratio between the standard deviation of wind speed and the mean speed (Stull, 1988), quantifies the turbulent energy within the flow. The integral length scale provides a measure of the average size of the largest turbulent eddy present within the flow (Kaimal and Finnigan, 1994). Meteorologists and building engineers have collected wind measurements over long time-scales, and report turbulence intensities of ~10-20% in urban terrain and over 50% at lower levels in cities (<10m), while integral length scales range from less than a meter to many tens of meters. More recently, wind measurements have been made in the ABL with higher temporal accuracy to gather information for surface vehicles and micro-air vehicles (MAVs). These measurements have shown that turbulence intensity relative to the moving vehicle varies from 7% (under light winds, < 5m/s) to >20% (under heavy winds > 5m/s), depending on wind, vehicle speed and terrain (Cooper and Watkins, 2007; Watkins et al., 2006; Wordley, 2009). When high levels of freestream turbulence are present within the ABL, wind speed and direction can change rapidly (Watkins et al., 2006), posing considerable challenges in terms of flight stability and control for flying animals that operate within the ABL.

Despite these challenges, many insects, birds and bats seem to be capable of contending with the adverse effects of freestream turbulence, likely through the use of both active and passive control strategies (Dickinson et al., 2000). However, our understanding of biological flight in natural flow conditions is limited, as most experiments on insect, bird and bat flight have been conducted in smooth flow or still air. Hummingbirds are ideal model organisms for studying the influence of complex wind environments on flight performance, as they are not only powerful flyers, but are also behaviorally amenable to performing consistent flights in controlled settings. Moreover, the high metabolic rate of hummingbirds (Suarez, 1992) makes them relentless foragers in a broad range of outdoor weather conditions, likely requiring them to utilize a variety of flight control strategies to contend with the airflow conditions they encounter in natural habitats. Recent studies have analyzed the dynamics of hummingbird flight in the unsteady von Kármán vortex street that forms behind a cylinder in flow (Ortega-Jimenez et al., 2013 & 2014). However, this type of flow is likely to be encountered only rarely in natural habitats (e.g., immediately downstream of an object in strong flow). In contrast, birds and other flying organisms are likely to encounter freestream turbulence

throughout most natural habitats whenever wind is present, making an assessment of their flight performance in turbulent flow conditions behaviorally and ecologically relevant.

In this study, we compared the position and orientation of the head, body and tail of ruby-throated hummingbirds, as well as their wing kinematics, while the hummingbirds maintained position at a feeder in both laminar and highly turbulent airflow. We created turbulence in a wind tunnel by placing a symmetric, planar grid at the inlet of the test section, generating flow conditions similar to those that hummingbirds would experience when foraging in a cluttered environment on a windy day, where wind passively interacts with obstacles (trees, leaves, etc.) to create freestream turbulence. The flow conditions generated here are fundamentally different from those utilized in previous experiments on flight in unsteady flows (Ortega-Jimenez et al., 2013 & 2014; Ravi et al., 2013), in which bumblebees, hawkmoths and hummingbirds were flown in the unsteady, structured flow present in the wake of a cylinder, where discrete alternating vortices are shed at a constant frequency. These structured wakes rapidly break down into the type of freestream turbulence generated in the present study, which consists of random variations in wind speed and direction that impose unpredictable perturbations at all frequencies and in all directions.

We compared the performance of hummingbirds flying in smooth and turbulent flow to address three main questions: (1) How does freestream turbulence influence stability of the hummingbird head and body during flight? (2) Are hummingbirds directionally sensitive to flow disturbances? And (3) What active and passive control strategies do hummingbirds employ to mitigate the effects of turbulence?

Results

Flow conditions

In both unimpeded and turbulent flow, a uniform velocity profile was present across the interrogation volume ($< 2\%$ variation in mean flow speed). With unimpeded flow, turbulence intensity in the wind tunnel test section was less than 1.2%. The integral length scale was not estimated for smooth flow, as it has limited significance at such low turbulence intensities. There were also no dominant velocity fluctuations at any particular frequency (Fig 2), indicating that the flow disturbance created by the small feeder upstream was minimal.

With the turbulence-generating grid present at the inlet of the test section, the turbulence intensity increased to 15% and the longitudinal integral length scale was 0.04 m. The power spectrum of turbulence showed no peak at any particular frequency and displayed an energy decay with a slope of $-5/3$ (black line in Fig. 2), which are distinguishing characteristics for fully mixed freestream turbulence (Pope, 2000). However, the turbulence generated here was not perfectly isotropic, as fluctuations along the lateral axis were slightly higher than those along the longitudinal and vertical axes (Table S1). This anisotropy is common for turbulence generated within wind tunnels, and considerable anisotropy also exists in the freestream turbulence in outdoor environments (Stull, 1988). The

integral length scale of the turbulence produced in the wind tunnel was on the order of the wing dimensions of the hummingbirds, which we hypothesize is likely to produce the greatest instabilities; disturbances many orders of magnitude greater than the wing dimensions would be experienced as quasi-steady changes in oncoming flow, and those many orders of magnitude smaller likely average out across the body to produce minimal disturbance.

Head and body stability

All hummingbirds were capable of maintaining remarkably constant head position with respect to the feeder across flow conditions, displaying fluctuations of < 1.5 mm when the mean wind speed was 5 m/s and the turbulence intensity was 15%. Turbulent flow did not appear to diminish the birds' ability to maintain head position, as there was no significant difference in the mean or standard deviation of the distance between the head and the feeder in smooth *versus* turbulent conditions (mean distance, $p = 0.59$; σ of distance, $p = 0.19$; Table S2). The head experienced greater translational accelerations (absolute values) along the lateral axis in turbulence as compared to smooth flow ($S-T_{lat}$, $p = 0.023$), but no statistically significant difference was noted in the accelerations between the two flow conditions along the longitudinal and vertical axes ($S-T_{long}$, $p = 0.62$; $S-T_{vert}$, $p = 0.99$; Fig. 3). The magnitude of head accelerations along each axis during flight in turbulence were not significantly different ($T_{long}-T_{lat}$, $p = 0.11$; $T_{long}-T_{vert}$, $p = 0.99$; $T_{lat}-T_{vert}$, $p = 0.07$). Roll, pitch and yaw rates (absolute values) of the head were generally quite small (Fig. 4), with significantly greater yaw rates in turbulent *versus* smooth flow conditions ($S-T_{yaw}$, $p = 0.037$). However, no significant difference in roll or pitch rates of the head were observed between flow conditions ($S-T_{roll}$, $p = 0.70$; $S-T_{pitch}$, $p = 0.06$).

In smooth flow, body accelerations were higher than those of the head along the lateral axis ($S_{lat_body}-S_{lat_head}$, $p = 0.014$), but head and body accelerations along the other axes were not significantly different ($S_{long_body}-S_{long_head}$, $p = 0.94$; $S_{vert_body}-S_{vert_head}$, $p = 0.26$). In contrast, turbulent flow resulted in body accelerations that were significantly greater than head accelerations along all three axes ($T_{lat_body}-T_{lat_head}$, $p = 0.03$; $T_{long_body}-T_{long_head}$, $p = 0.04$; $T_{vert_body}-T_{vert_head}$, $p = 0.005$; Fig. 3). In addition, body accelerations along the lateral axis were significantly greater than those along the longitudinal or vertical axes during flight in turbulence ($T_{lat}-T_{long}$, $p = 0.040$; $T_{lat}-T_{vert}$, $p = 0.08$; $T_{long}-T_{vert}$, $p = 0.002$). Across flow conditions, body accelerations were significantly greater along all axes in turbulent flow as compared to smooth flow ($S-T_{lat}$, $p = 0.03$, $S-T_{long}$, $p = 0.027$ & $S-T_{vert}$, $p = 0.042$).

In turbulent flow, absolute rotation rates of the body along all three axes were significantly higher than those of the head ($T_{roll_body}-T_{roll_head}$, $T_{pitch_body}-T_{pitch_head}$ & $T_{yaw_body}-T_{yaw_head}$, $p < 0.008$), and body rotation rates were significantly higher in turbulence as compared to smooth flow ($S-T_{roll}$, $p = 0.0054$, $S-T_{pitch}$, $p = 0.048$ & $S-T_{yaw}$, $p = 0.019$; Fig. 4). In addition, roll rates of the body were significantly

greater than pitch or yaw rates during flight in turbulent conditions ($T_{roll}-T_{pitch}$, $p = 0.001$; $T_{roll}-T_{yaw}$, $p = 0.007$; $T_{pitch}-T_{yaw}$, $p = 0.21$).

Tail kinematics and body forces

Tail kinematics data show that the tail does not move significantly more than the body in smooth flow, with no significant difference in roll, pitch or yaw rates between the tail and body ($S_{roll_tail}-S_{roll_body}$, $p = 0.47$; $S_{pitch_tail}-S_{pitch_body}$, $p = 0.15$; $S_{yaw_tail}-S_{yaw_body}$, $p = 0.15$; Fig. 4). However, in turbulent flow, pitch rates of the tail were significantly higher than those of the body ($T_{pitch_tail}-T_{pitch_body}$, $p = 0.065$), whereas roll and yaw rates were not significantly different ($T_{roll_tail}-T_{roll_body}$, $p = 0.13$; $T_{yaw_tail}-T_{yaw_body}$, $p = 0.18$). Tail rotation rates in turbulence were significantly higher than tail rotation rates in smooth flow ($S-T_{roll}$, $p = 0.02$, $S-T_{pitch}$, $p = 0.03$ & $S-T_{yaw}$, $p = 0.02$), and did not differ significantly between the three axes ($T_{roll}-T_{pitch}$, $p = 0.65$; $T_{roll}-T_{yaw}$, $p = 0.13$; $T_{pitch}-T_{yaw}$, $p = 0.40$; Fig. 4). Hummingbirds also increased the mean fan angle of their tails significantly when flying in turbulence ($p = 0.04$; Fig. 5a), and fan angle was significantly more variable in turbulent *versus* smooth flow ($p = 0.007$; Fig. 5b).

Force measurements performed on a static hummingbird body in smooth flow revealed that variations in tail position and fan angle affect the lift and drag produced by the body. For both body angles investigated here (0° & 20°), increasing the tail fan angle and depressing the tail (i.e. increasing tail pitch angle relative to the body), as was observed during flight in turbulence, increased both lift and drag generated by the body (Fig. 6). For both body angles, more lift was generated by fanning the tail (with or without changing its pitch) than by depressing the tail without fanning. Lift was enhanced more at the higher body angle (20°). Conversely, more drag was generated by depressing the tail (with or without fanning) than by fanning it with no change in pitch angle. Drag increased more at the lower body angle (0°). Tail fanning always resulted in an increase in lift and drag but its influence was more pronounced at lower body angles. Maximum lift and drag, therefore, occurred with the tail depressed and the tail feathers fanned out.

Wing kinematics

Large variations in flapping frequency, stroke amplitude and stroke plane angle from one wingbeat to the next were observed when hummingbirds flew in turbulent conditions (Fig. 7g-h, supplementary video 1&2). Mean flapping frequency was higher in turbulent flow ($p = 0.0065$; Table S2), but the increase in frequency was only marginal compared to smooth flow, the flapping frequency was also significantly more variable (higher σ) in turbulent *versus* smooth flow ($p = 0.008$; Table S2). Mean stroke amplitude was significantly higher in turbulent *versus* smooth flow ($p = 0.046$; Fig. 7a), and significantly more variable ($p = 0.042$; Fig. 7b). Birds flying in turbulent air adopted a higher mean stroke plane angle relative to their body angle ($p = 0.046$; Fig. 7d), which was more variable from one stroke to the next in turbulent *versus* smooth flow ($p = 0.02$; Fig. 7e). In addition to varying their kinematics from one stroke to the next, hummingbirds flying in turbulent flow increased the asymmetry of their wing strokes, with larger left-right differences in stroke amplitude ($p = 0.034$; Fig. 7c) and stroke plane angle ($p = 0.025$; Figs. 7f) compared to smooth flow.

The birds' maximal capacity to vary left *versus* right wing kinematics (stroke plane angle and stroke amplitude) is reported in Table S2 as the maximum bilateral difference in each kinematic variable. The

birds were able to render large bilaterally asymmetric changes in both variables, with greater left:right asymmetries occurring during flight in turbulent flow. The asymmetric variations in left *versus* right wing stroke plane angle and stroke amplitude did not occur in phase, as the standard deviations of bilateral asymmetry in these variables were greater than the standard deviations observed for either left *versus* right wing individually (Table S2).

Discussion

Effects of unsteady flow on flight stability

Unsteady wind is ubiquitous in natural habitats, and its complex and unsteady properties can render the aerial environment challenging for flying organisms. In the highly turbulent flow environment generated here, the hummingbirds' heads were likely subjected to translational and rotational disturbances induced by both the unsteady wind and by disturbances propagated from the body to the head, through the neck. Given these imposed perturbations, the hummingbirds maintained remarkably stable head position and orientation, displaying <1.5 mm fluctuations in head position while flying in relative turbulence intensities that would ground most current Micro-Air Vehicles (Abdulrahim et al., 2010; Watkins et al., 2009), see supplementary video 1&2. Accelerations of the head were nearly two orders of magnitude lower than those present in the oncoming flow (see Fig. 3), and head rotation rates were minimal, typically <0.5 revolutions/sec. The head stability of birds, in steady flight or while maneuvering, has been studied and reported in previous investigations (Erichsen et al., 1989; Land, 1999; Warrick et al., 2002; Ros and Biewener 2015, in review), and birds have been shown to rely upon their ocular and vestibular reflexes to maintain a stable head orientation as their body undergoes rotations and translations (Erichsen et al., 1989; Warrick et al., 2002; Ros, 2013). The translational and rotational disturbances induced by the turbulent flow interacting directly with the hummingbird's head were likely small, due to the relatively small size and streamlined profile of the head. The limited variations in the head position and orientation observed here could also be due to the birds' desire to continue feeding and thus higher variations may be present when foraging at a distance from food sources. However, the hummingbird's body does experience considerably larger fluctuations in position and orientation, and the bird's neck appears to effectively attenuate and damp these variations (Figs 3, 4a-b), as has been observed when hummingbirds track artificial visual surrounds (Ros, 2013; Ros and Biewener 2015, in review).

When flying in turbulent conditions, the hummingbird's body undergoes accelerations and rotations that are nearly twice as large as those observed in the head (Figs. 3, 4), with the greatest translational disturbances occurring along their mediolateral axis and the greatest rotational disturbances about their roll axis (Figs. 3, 4), see supplementary video 1&2. Similar results have been obtained for hummingbirds and bumblebees flying in unsteady vortex streets (Ortega-Jimenez et al., 2014; Ravi et al., 2013), whereas hawkmoths flying in vortex streets display greater instability in yaw than in roll

(Ortega-Jimenez et al., 2013). Instantaneous variations in position and orientation of the body are likely due to a complex combination of drag-based interactions with the unsteady airflow, force and moment imbalances on the wings and tail due to the heterogeneous flow environment, and active reorientation performed by the birds to compensate for perturbations.

Some attenuation of the disturbances induced by unsteady airflow is expected due to the bird's own inertia, which would reduce translational motions equally in all directions, but inhibit pitch and yaw rotations more effectively than roll rotations (due to the lower moment of inertia around this axis). However, hummingbirds undoubtedly also responded actively to the aerial perturbations via changes in wing and tail kinematics, including both dynamic adjustments (reflected by increased variability) and fixed shifts (reflected by altered mean values). We were not able to estimate the relative contributions of external airflow perturbations *versus* active compensatory responses to the observed body motions in this study, due to the lack of information on instantaneous wind profile, activation of muscles involved in flight control, and instantaneous forces generated by the wings and body. Visualizing the wind profile around a freely flying bird in unpredictable, turbulent flow is challenging and would require instantaneous 3D particle image velocimetry. Assessing time-varying forces produced by the wings and body through active muscle control would be equally challenging. The future development of techniques to perform these types of measurements would improve our understanding of the physical and neuromuscular processes underlying hummingbirds' remarkable flight stability in unsteady flows.

Compensatory turbulence mitigation strategies

Our results suggest that hummingbirds flying in turbulent flow compensate for aerial perturbations by employing instantaneous adjustments (reflected by increased stroke to stroke variability and bilateral asymmetry; Fig. 7), as well as longer-term, fixed changes in kinematic parameters (reflected by altered mean values; Figs. 7a, d), which may improve passive stability and reduce the need for instantaneous compensation. Wing beat frequency increased slightly in turbulence (~3% increase, though this trend was not statistically significant), and became significantly more variable from beat to beat. Previous studies have shown that hummingbirds display statistically significant but modest increases in flapping frequency to increase force production during hovering (~4-10% increase in reduced air density or up to 19% with added loads - Chai and Dudley, 1995; Altshuler and Dudley, 2003) and while flying in the unsteady wake behind a cylinder (~10% increase, Ortega-Jimenez et al., 2014), but display no significant change in frequency with increased flight speeds in smooth flow (Tobalske et al., 2007). Hummingbirds flying in unsteady vortex streets also display increased variability in flapping frequency (Ortega-Jimenez et al., 2014), as in our study.

When flying in turbulent flow, the hummingbirds also displayed a significant, but fairly modest (~7%) increase in mean stroke amplitude, as well as greater stroke-to-stroke variability and bilateral asymmetry. Previous studies have shown that hummingbirds increase stroke amplitude to maximize force production when hovering with loads or in variable-density gases (~19-24% - Chai and Dudley, 1995; Altshuler and Dudley, 2003), and at higher flight speeds (e.g., ~25% increase from 8 to 12 m/s;

Tobalske et al., 2007). When flying in the unsteady wake behind a cylinder, hummingbirds do not increase mean stroke amplitude, but variability and bilateral asymmetry in amplitude increase significantly (Ortega-Jimenez et al., 2014). Thus, our data show that hummingbirds flying in fully mixed, freestream turbulence display some of the same kinematic adjustments in stroke amplitude as those seen during flight in unsteady vortex streets (increased variability and bilateral asymmetry), as well as those seen when hummingbirds increase force production during hovering or forward flight (increased mean amplitude).

Anatomical stroke plane angle (stroke plane relative to the body) increased significantly and became more variable in turbulent airflow. Hummingbirds flying in laminar flow have previously been shown to maintain a fixed anatomical stroke plane angle while decreasing body angle as flight speed increases from hovering to 6 m/s, but to increase anatomical stroke plane angle at flight speeds greater than 8 m/s (Tobalske et al., 2007). Here, we found an approximately 20% increase in anatomical stroke plane angle during flight in turbulent *versus* smooth flow at 5 m/s, comparable in magnitude to the change in anatomical stroke plane angle from 6 to 12 m/s in laminar flow (Tobalske et al., 2007). We also found an increase in bilateral asymmetry of stroke plane angle during flight in turbulent air.

The aerodynamic role of the tail in avian flight has been the subject of much debate, with various hypotheses proposed concerning the underlying aerodynamic mechanisms of force production by the tail (Evans et al., 2002; Maybury et al., 2001; Thomas, 1993). Our findings suggest that the tail of the hummingbird likely plays an important role in improving flight stability in complex aerial environments. The large pitch and yaw rotation rates of the tail in turbulent airflow almost certainly reflect a combination of passive interactions with the imposed airflow and active compensatory rotations produced by the hummingbirds to correct for perturbations. Consistent with this interpretation, tail pitch angle has previously been shown to be more variable during flight in vortex streets as well (Ortega-Jimenez et al., 2014).

Apart from rapidly changing the orientation of the tail, our data also show that hummingbirds increase the mean fan angle of their tails and display higher variability in fan angle during flight in turbulence. Limited information exists on the aerodynamic function of tail fanning or on its role in flight stabilization. The observed increase in mean fan angle may improve passive stability by increasing the surface area of the tail, enhancing passive damping of aerial disturbances. Su et al. (2012) reported that passerines fan their tail to recover from downward pitching moments experienced during the downstroke; however a similar relationship with the stroke cycle was not noted here. An increased tail fan angle also leads to greater lift production (Fig. 6; Maybury et al., 2001), which would reduce the aerodynamic demands on the wings, potentially providing birds with higher control authority to employ in turbulence mitigation. The increased variability in tail fan angle also suggests that tail fanning may be used to perform or enhance rapid corrective maneuvers. Consistent with this interpretation, we observed several instances of rapid changes in tail fanning angle that were correlated with large changes in body orientation, Fig. S8.

Overall, our results show that hummingbirds employ both dynamic and fixed changes in several kinematic variables during flight in turbulent *versus* smooth flow. Increases in mean stroke amplitude, anatomical stroke plane angle and tail fanning angle may all serve to increase aerodynamic force production and/or improve passive stability. The hummingbirds also displayed increased stroke to stroke variability in nearly every kinematic parameter measured when flying under highly turbulent conditions – including increased variability of flapping frequency, stroke amplitude, anatomical stroke plane angle, tail rotation rates, and tail fanning angle. Finally, the hummingbirds also displayed increased bilateral asymmetry in stroke amplitude and stroke plane angle. Taken together, these changes suggest that hummingbirds actively respond to compensate for aerial perturbations imposed by turbulent flow via a variety of mechanisms.

Energetic considerations for flight in turbulence

Although hummingbirds are clearly capable of contending with high levels of turbulence by employing a variety of kinematic mechanisms, the feasibility and likelihood of wild hummingbirds actually flying in adverse wind conditions is likely influenced by the metabolic costs associated with these adjustments. Body force measurements taken at different tail configurations indicate that the increased fan angle maintained by ruby-throated hummingbirds while flying in turbulence incurs a drag penalty (Fig. 6). The hummingbirds also displayed modest increases in both flapping frequency and stroke amplitude, which suggest an increased energetic cost. However, when flying in the unsteady wake behind a cylinder, Anna's hummingbirds (*C. anna*) display no change in metabolic rate as compared to flight in smooth flow, until flight speeds reach 9 m/s (Ortega-Jimenez et al., 2014), suggesting that Anna's hummingbirds, and perhaps also ruby-throated hummingbirds, have high tolerance to variations in the aerial environment without significant energetic penalty. However, whereas some of the kinematic changes we observed in ruby-throated hummingbirds flying in turbulence are similar to those seen in Anna's hummingbirds flying in the wake of a cylinder (e.g., modest increases in flapping frequency and increased variability in frequency and amplitude), we also observed kinematic changes that are associated with high speed flight (e.g., increased mean stroke amplitude and increased anatomical stroke plane angle). Both high speed and maneuvering flight are associated with changes in wing kinematic variables, such as an increase in stroke amplitude, which have been shown to incur greater energetic costs (Clark and Dudley, 2010). Our finding that many of these kinematic changes also occur during flight in turbulent flow, whereas they are absent during flight behind a vortex street, suggests that flying in fully mixed turbulence may be more energetically demanding than flying in the unsteady, structured wakes of objects. Future studies involving respirometry measurements of hummingbirds flying in turbulent *versus* smooth flow and measurements of top flight speeds in these flow conditions would provide more direct information about the energetic costs and limits of hummingbird flight in freestream turbulence, the flow condition that hummingbirds are likely to encounter most frequently in natural habitats.

Materials and Methods

Animals and flight tests

Four female ruby-throated (*Archilochus colubris*) hummingbirds were caught in Bedford, MA and maintained at the Concord Field Station for up to one week prior to experiments. Birds were housed in 0.5 x 0.5 x 0.5 m husbandry flight chambers where they were provided *ad libitum* access to fortified nectar solution (Nektar Plus, Nekton USA) in a hummingbird feeder. Experiments were conducted once birds were sufficiently acclimatized to their captive environment. Immediately prior to experiments, each bird was held gently while markers were placed on the head, beak, torso and wings. The markers on the head consisted of two small black dots separated by 10 mm; markers on the torso consisted of three black points representing the vertices of an isosceles triangle (measuring 2.7 x 2.3 mm). All markers were set upon a white background (Fig. 1), and were affixed using cyanoacrylate glue. Small dots of reflective white paint were placed on the beak and on the leading edge of each wing, around the midpoint of the span (Fig 1).

Each bird was then released into the test section of the wind tunnel, which contained a small 1 ml tuberculin syringe filled with sucrose solution located 800 mm from the inlet of the test section, as well as a perch in the downstream end. All birds began feeding within a minute of being released in the wind tunnel. Once birds were sufficiently calm and began feeding consistently, wind speed in the tunnel was increased. During flight trials, birds maintained position while feeding from the tuberculin syringe (sustaining a forward flight speed of ~5 m/s), and were filmed using two Photron SA3 high-speed cameras sampling at 1000 Hz, placed above the wind tunnel at approximately 30° from the vertical. A static calibration cube that filled the volume of interest was used for spatial calibration via direct linear transformation (Hedrick, 2008).

Experiments were conducted in a 6 m long, suction-type, open-return wind tunnel with a 1.5 L x 0.5 W x 0.5 H m working section. Wind-speed was set to ~5 m/s, which represents an intermediate cruising velocity for hummingbirds (Tobalske et al., 2007). To generate fully mixed freestream turbulence, a symmetric planar grid was introduced at the inlet of the test section. The grid consisted of panels of 40 mm width and 40 mm inter-panel spacing (Fig. 2). These dimensions were chosen because they resulted in the highest level of fully mixed turbulence intensity within the wind tunnel. The interaction between airflow and the grid results in the formation of discrete vortices immediately downstream of the panel (Comte-Bellot and Corrsin, 1966), which advect downstream and eventually break down to form fully mixed freestream turbulence (Batchelor and Townsend, 1948) due to viscosity and interactions between vortices. The region of interest in these experiments was located approximately 20 panel widths downstream from the grid, which is the distance generally required for discrete vortices to break down to fully mixed turbulence (Mohamed and Larue, 1990; Gad-El-Hak and Corrsin, 1974). Fluctuations in flow velocity within the wind tunnel were quantified using a three component hot-wire anemometer (55P91 probe, Dantec Dynamics, Sweden) sampling at 1kHz, calibrated against a standard pitot-static tube.

We characterized the level of turbulence generated by calculating the turbulence intensity (standard deviation of wind speed/mean wind speed) and the integral length scale. In this study, the auto-correlation method was used to estimate the integral length scale along the longitudinal axis (see Ravi, 2011 for further details).

Kinematics reconstruction and analysis

Recorded flight sequences were digitized using an open-source MATLAB-based routine, DLTdv5 (Hedrick, 2008). In addition to digitizing all markers, the shoulder joints (where the wings attach to the thorax), base of the tail (midline of where the tail meets the body), and extremities of the tail (tips of the outermost tail feathers) were also digitized (Fig. 2, blue dots), for a total of 12 points digitized over 0.5 s of flight (20-22 wingbeats) for each bird. Subsequent kinematic analyses were performed in MATLAB.

Digitization error in localizing the centroids of marker points was estimated to be approximately 1-2 pixels, which was much smaller than the mean number of pixels separating the markers (~50). This error is expected to manifest only at higher frequencies, on the order of the Nyquist frequency. To remove any higher frequency errors due to the digitization process, position data were passed through a 4th order, low-pass Butterworth filter with a cutoff frequency of 400 Hz, which is lower than the Nyquist frequency (500 Hz) but higher than the flapping frequency of the birds (~45 Hz). To examine motions that occur over timescales greater than one wingbeat, we further filtered calculated accelerations and rotations of the head, body and tail with a 30 Hz low-pass filter (4th order Butterworth) to remove motions due to the flapping wings. Reconstructed wing kinematics were passed through a 4th order, low-pass Butterworth filter with a cutoff frequency of 200 Hz to further smooth the wing trajectories.

Instantaneous velocities and accelerations of the head and body were calculated by taking time derivatives of the positions. Translational accelerations of the head and body were calculated in a global coordinate system based on the wind tunnel's working section (longitudinal = long axis of the wind tunnel/direction of mean flow, lateral and vertical span the cross-section in the horizontal and vertical directions, respectively). For calculating roll, pitch and yaw of the head and body, a local plane was constructed based on the three marker points present on each body segment (triangular marker for torso and two head markers + beak marker for head). Assuming rigid body dynamics, the instantaneous orientation and rotation rates of these planes were calculated using the method detailed previously (Ravi et al., 2013). The instantaneous orientation of the head was calculated with respect to the global coordinate system, while the orientation of the torso was calculated with respect to the local coordinate system of the head. The orientation of the tail was determined by constructing a local tail plane, formed by the base and extremities of the tail, and calculating the orientation of this plane with respect to the local coordinate system of the torso (using the method described in Ravi et al., 2013). The fan angle of the tail was calculated as the angle between the vectors connecting the

extremities of the tail to the tail base. The fan angle was measured at each frame for the entire flight sequence recorded, the mean and standard deviation of the same over the flight was measured and compared in smooth and turbulent wind conditions.

Because a constant and stable head position is assumed to improve feeding efficiency, feeding performance was assessed by measuring the distance between the beak and the feeder over the course of each flight trial. The magnitude of fluctuations (standard deviation) in this distance was compared across smooth and turbulent flow conditions. Mean absolute values of translational accelerations and rotation rates of the head were calculated with respect to the global coordinate system and compared across flow conditions. A similar analysis was performed to assess stability of the torso in laminar and turbulent flow, whereby the mean absolute value of translational accelerations and rotation rates along each axis of the body were compared. To assess tail deployment as a potential flight control mechanism, roll, pitch and yaw angles of the tail were calculated with respect to the local coordinate system of the torso, and mean absolute rotation rates of the tail were compared between the two flow conditions. In addition, the use of tail fanning as a potential control mechanism was investigated by calculating the mean and standard deviation of fan angle during flight in laminar *versus* turbulent flow.

Wing kinematics were derived from the digitized positions of the shoulder joints and the leading edge markers on each wing. For each stroke, the flapping frequency was calculated as the inverse of the wing beat period, which was independently measured on the left and right wing and then averaged. The wingbeat frequency at each stroke was subsequently averaged over the recorded sequence to estimate the mean flapping frequency in smooth and turbulent wind. The standard deviation of the flapping frequency over the recording was compared between the two flow conditions. Stroke amplitude was measured as the angle swept by the leading edge with respect to the wing base between the top of the upstroke and bottom of the downstroke, and was calculated for the left and right wings separately during each stroke. The mean and standard deviation of the stroke amplitude of the birds in the two wind conditions over entire recording was compared. The anatomical stroke plane angle was calculated for each wingbeat by estimating the pitch angle between the body and a 2D regression line of the position of the leading edge throughout a stroke projected onto the x-y plane; this procedure was conducted separately for each wing. The mean and standard deviation of the anatomical stroke-plane angle was also taken over the entire sequence and compared between smooth and turbulent wind conditions. Stroke plane amplitude and anatomical stroke plane angle were independently measured for the left and right wings to examine how mean values and stroke-to-stroke bilateral variability differed between smooth and turbulent flow. To assess bilateral asymmetry in these variables, the difference between the left and right wing was calculated for each stroke. Subsequently the standard deviation of the stroke-resolve bilateral asymmetry in amplitude and stroke-plane angle was calculated over the entire sequence.

Statistical significance of results was analyzed by performing a parametric repeated measures ANOVA test ($n = 4$ individuals in all cases) between experimental conditions (smooth flow [S], turbulent [T]), or between pairs of translational (Long.-Lat., Long.-Vert. & Lat.-Vert.) or rotational axes (Roll-Pitch, Roll-Yaw & Pitch-Yaw) in MATLAB.

Body force measurements

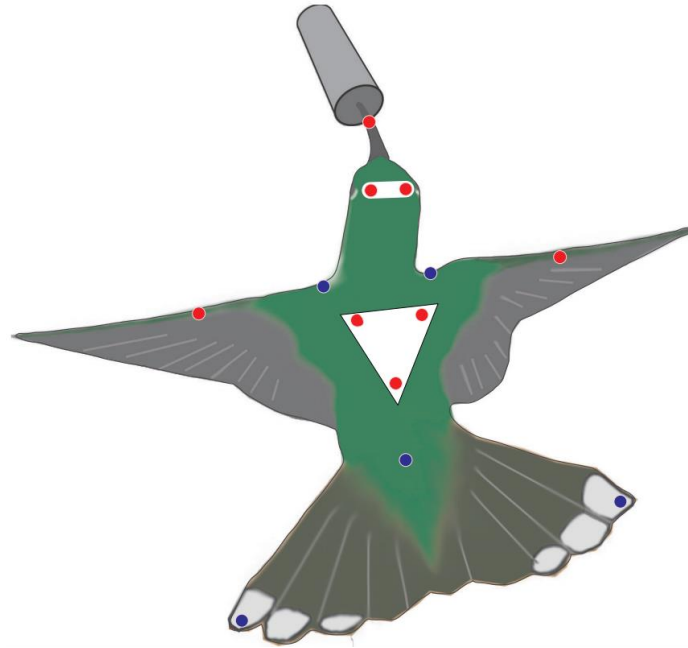
To test the effects of observed changes in body and tail orientation, we measured the forces generated by a static hummingbird body in various configurations, placed in the wind tunnel with laminar flow. The wings of a euthanized hummingbird were removed and the body was attached to an ATI Nano17 force balance (ATI Industrial Automation, Apex NC) via a thin carbon fiber rod. The rod was placed near the estimated location of the center of gravity of the body (posterior and ventral to the wing hinge). Because the rod was small, its influence on airflow and the resulting forces was judged to be negligible. Lift and drag forces were assumed to act perpendicular and parallel to the mean wind direction, respectively. A wire support placed along the longitudinal axis of the body was used to vary the pitch of the body and tail. Different tail fan angles were set using a wire support glued laterally across the basal part of the tail. Forces generated by the hummingbird body were measured at 0° and 20° body pitch angle with respect to the oncoming wind, which were typical orientations within the range maintained by the birds in free flight. Tail pitch and fan angles were altered to examine force production at the extreme values of these variables measured in free flight. Thus, for each body angle, forces were measured with a tail pitch of 0° or 20° (tail down) with respect to the body, and for each body and tail orientation, tail fan angle was set to 53° (unfanned) or 104° (fanned).

References

- Abdulahim, M., Watkins, S., Segal, R., Marino, M. and Sheridan, J.** (2010). Dynamic Sensitivity to Atmospheric Turbulence of Unmanned Air Vehicles with Varying Configuration. *J. Aircr.* **47**, 1873–1883.
- Altshuler, D. L. and Dudley, R.** (2003). Kinematics of hovering hummingbird flight along simulated and natural elevational gradients. *J. Exp. Biol.* **206**, 3139–47.
- Batchelor, G. K. and Townsend, A. A.** (1948). Decay of Turbulence in the Final Period. *Proc. R. Soc. A Math. Phys. Eng. Sci.* **194**, 527–543.
- Chai, P. and Dudley, R.** (1995). Limits to vertebrate locomotor energetics suggested by hummingbirds hovering in heliox. *Nature* **377**, 722–725.
- Clark, C. J. and Dudley, R.** (2010). Hovering and forward flight energetics in Anna's and Allen's hummingbirds. *Physiol. Biochem. Zool.* **83**, 654–62.
- Comte-Bellot, G. and Corrsin, S.** (1966). The use of a contraction to improve the isotropy of grid-generated turbulence. *J. Fluid Mech.* **25**, 657–682.
- Cooper, K. R. and Watkins, S.** (2007). The Unsteady Wind Environment of Road Vehicles, Part One: A Review of the On-road Turbulent Wind Environment. In *Vehicle Aerodynamics 2007*, pp. 315–332. Warrendale PA, USA: Society of Automotive Engineers.

- 488 **Dickinson, M. H., Farley, C. T., Full, R. J., Koehl, M. A., Kram, R. and Lehman, S.** (2000). How animals
489 move: an integrative view. *Science* **288**, 100–6.
- 490 **Erichsen, J. T., Hodos, W., Evinger, C., Bessette, B. B. and Phillips, S. J.** (1989). Head Orientation in
491 Pigeons: Postural, Locomotor and Visual Determinants. *Brain. Behav. Evol.* **33**, 268–278.
- 492 **Evans, M. R., Rosén, M., Park, K. J. and Hedenström, A.** (2002). How do birds' tails work? Delta-wing
493 theory fails to predict tail shape during flight. *Proc. Biol. Sci.* **269**, 1053–7.
- 494 **Gad-El-Hak, M. and Corrsin, S.** (1974). Measurements of the nearly isotropic turbulence behind a
495 uniform jet grid. *J. Fluid Mech.* **62**, 115–143.
- 496 **Hedrick, T. L.** (2008). Software techniques for two- and three-dimensional kinematic measurements of
497 biological and biomimetic systems. *Bioinspir. Biomim.* **3**, 034001.
- 498 **Kaimal, J. C. and Finnigan, J. J.** (1994). *Atmospheric Boundary Layer Flows: Their Structure and*
499 *Measurement*. Oxford University Press, USA.
- 500 **Land, M. F.** (1999). The roles of head movements in the search and capture strategy of a tern (Aves,
501 Laridae). *J. Comp. Physiol. A Sensory, Neural, Behav. Physiol.* **184**, 265–272.
- 502 **Maybury, W. J., Rayner, J. M. and Couldrick, L. B.** (2001). Lift generation by the avian tail. *Proc. Biol.*
503 *Sci.* **268**, 1443–8.
- 504 **Mohamed, M. S. and Larue, J. C.** (1990). The decay power law in grid-generated turbulence. *J. Fluid*
505 *Mech.* **219**, 195–214.
- 506 **Ortega-Jimenez, V. M., Greeter, J. S. M., Mittal, R. and Hedrick, T. L.** (2013). Hawkmoth flight stability
507 in turbulent vortex streets. *J. Exp. Biol.* **216**, 4567–79.
- 508 **Ortega-Jimenez, V. M., Sapir, N., Wolf, M., Variano, E. A. and Dudley, R.** (2014). Into turbulent air:
509 size-dependent effects of von Kármán vortex streets on hummingbird flight kinematics and
510 energetics. *Proc. Biol. Sci.* **281**, 20140180.
- 511 **Pope, S. B.** (2000). *Turbulent Flows*. Cambridge University Press.
- 512 **Ravi, S.** (2011). The Influence of Turbulence on a Flat Plate Airfoil at Reynolds Numbers Relevant to
513 MAVs. Ph.D. Thesis. RMIT University
- 514 **Ravi, S., Crall, J. D., Fisher, A. and Combes, S. A.** (2013). Rolling with the flow: bumblebees flying in
515 unsteady wakes. *J. Exp. Biol.* **216**, 4299–309.
- 516 **Ros, I. G.** (2013). *Low Speed Avian Maneuvering Flight*. Ph.D. Thesis. Harvard University
- 517 **Ros, I. G. and A. A. Biewener** (in review) Optic flow stabilizes flight in Ruby-throated hummingbirds. *J.*
518 *Exp. Biol.*

- 519 **Stull, R. B.** (1988). *An Introduction to Boundary Layer Meteorology*. (ed. Stull, R. B.) Dordrecht:
520 Springer Netherlands.
- 521 **Su, J.-Y., Ting, S.-C., Chang, Y.-H. and Yang, J.-T.** (2012). A passerine spreads its tail to facilitate a rapid
522 recovery of its body posture during hovering. *J. R. Soc. Interface* **9**, 1674–84.
- 523 **Suarez, R. K.** (1992). Hummingbird flight: Sustaining the highest mass-specific metabolic rates among
524 vertebrates. *Experientia* **48**, 565–570.
- 525 **Thomas, A. L. R.** (1993). On the Aerodynamics of Birds' Tails. *Philos. Trans. R. Soc. B Biol. Sci.* **340**, 361–
526 380.
- 527 **Tobalske, B. W., Warrick, D. R., Clark, C. J., Powers, D. R., Hedrick, T. L., Hyder, G. A. and Biewener,**
528 **A. A.** (2007). Three-dimensional kinematics of hummingbird flight. *J. Exp. Biol.* **210**, 2368–2382.
- 529 **Warrick, D. R., Bundle, M. W. and Dial, K. P.** (2002). Bird maneuvering flight: blurred bodies, clear
530 heads. *Integr. Comp. Biol.* **42**, 141–8.
- 531 **Watkins, S., Milbank, J., Loxton, B. J. and Melbourne, W. H.** (2006). Atmospheric Winds and Their
532 Implications for Microair Vehicles. *AIAA J.* **44**, 2591–2600.
- 533 **Watkins, S., Abdulrahim, M., Thompson, M., Shortis, M., Segal, R. and Sheridan, J.** (2009). An
534 Overview of Experiments on the Dynamic Sensitivity of MAVs to Turbulence.
- 535 **Wordley, S. J.** (2009). On-Road Turbulence. Ph.D. Thesis. Monash University
- 536
- 537



538

539

540

Fig. 1: Schematic showing the points digitized on the hummingbird. Red points represent markers of reflective paint applied to the bird, and blue points represent biological landmarks that were estimated visually.

541

542

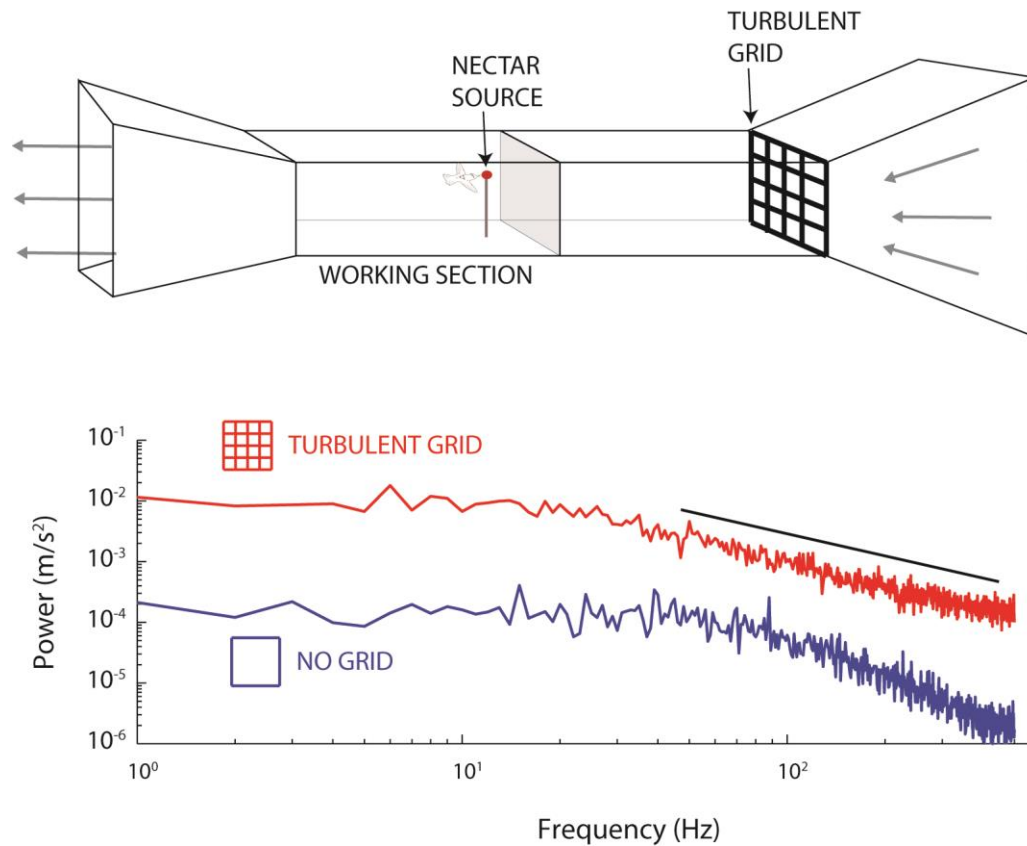


Fig. 2: (A) Schematic of the wind tunnel with a planar turbulence grid placed at the inlet of the test section. A screen (gray square) was placed upstream of the nectar source to prevent the birds from flying into the contraction section of the wind tunnel, and all airflow measurements were taken downstream of the screen and feeder. (B) Power spectral density of velocity fluctuations in smooth and turbulent wind conditions. Black line indicates a slope of $-5/3$, a distinguishing characteristic for fully mixed freestream turbulence.

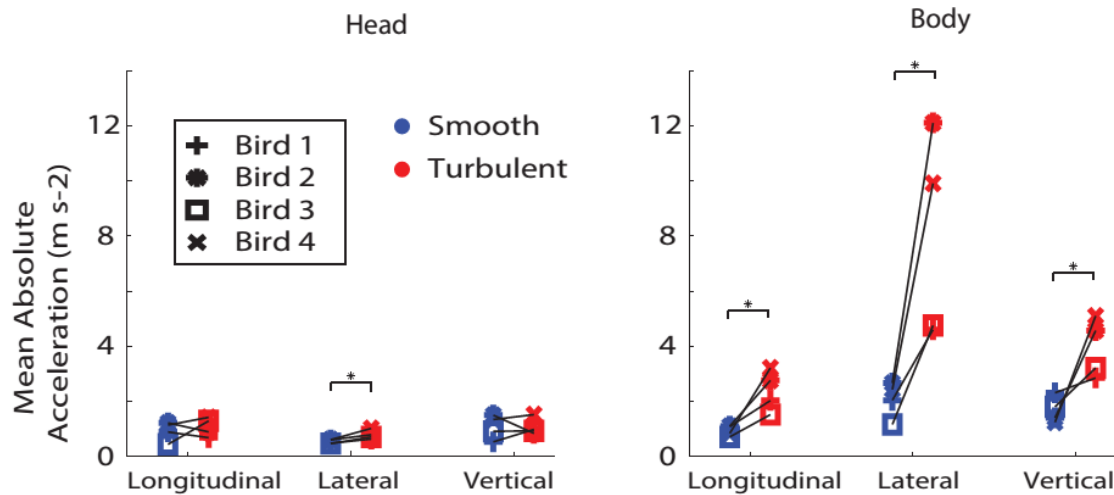


Fig. 3: Mean absolute accelerations experienced by (A) the head and (B) the body of hummingbirds along the longitudinal, lateral and vertical directions of the wind tunnel in smooth (blue) and turbulent (red) flow conditions.

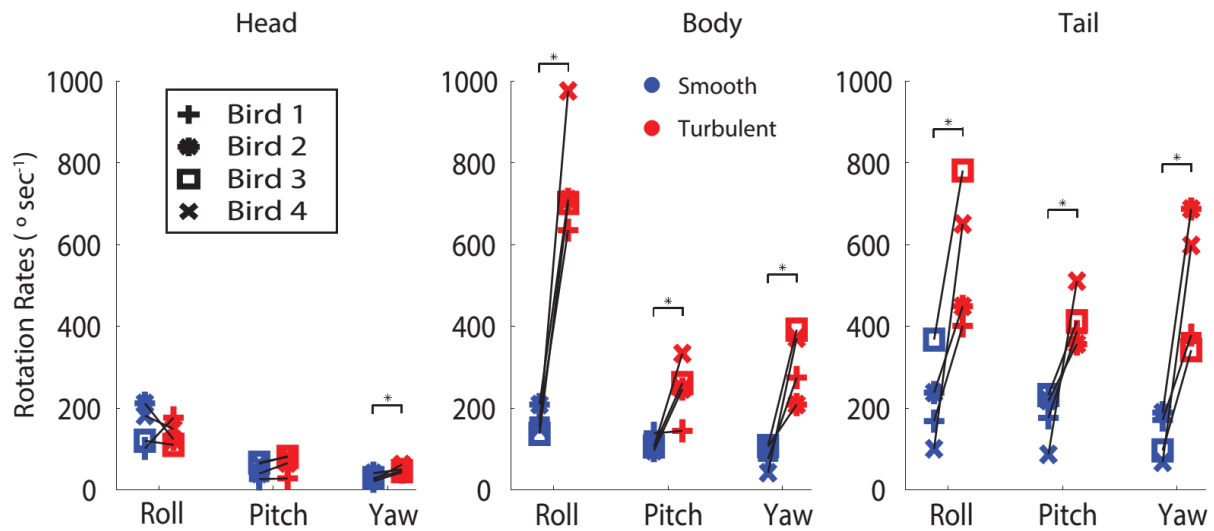


Fig. 4: Mean absolute rotation rates experienced by (A) the head, (B) the body, and (C) the tail of hummingbirds along the roll, pitch and yaw axes, in smooth (blue) and turbulent (red) flow conditions.

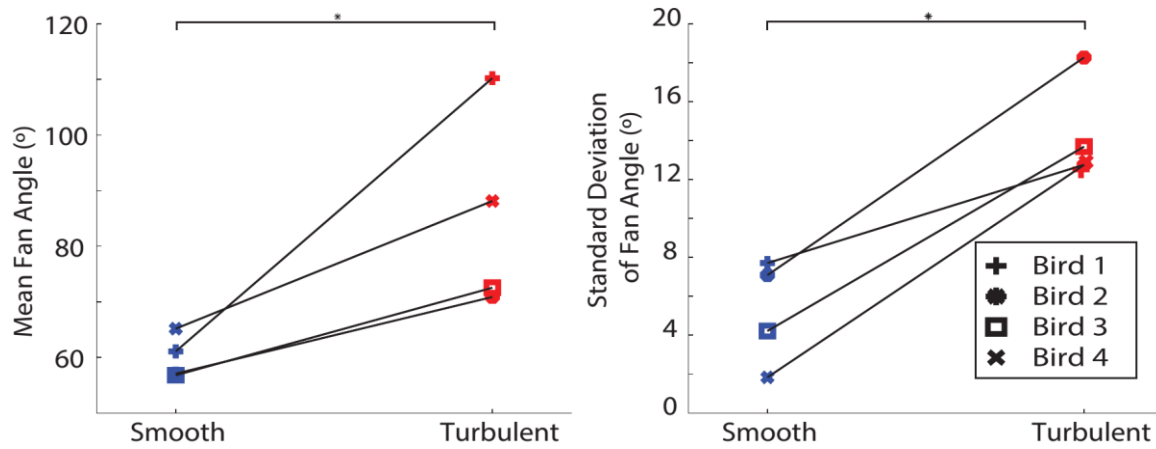


Fig. 5: (A) Mean and (B) standard deviation (σ) of tail fan angles for hummingbirds flying in smooth (blue) and turbulent (red) flow conditions.

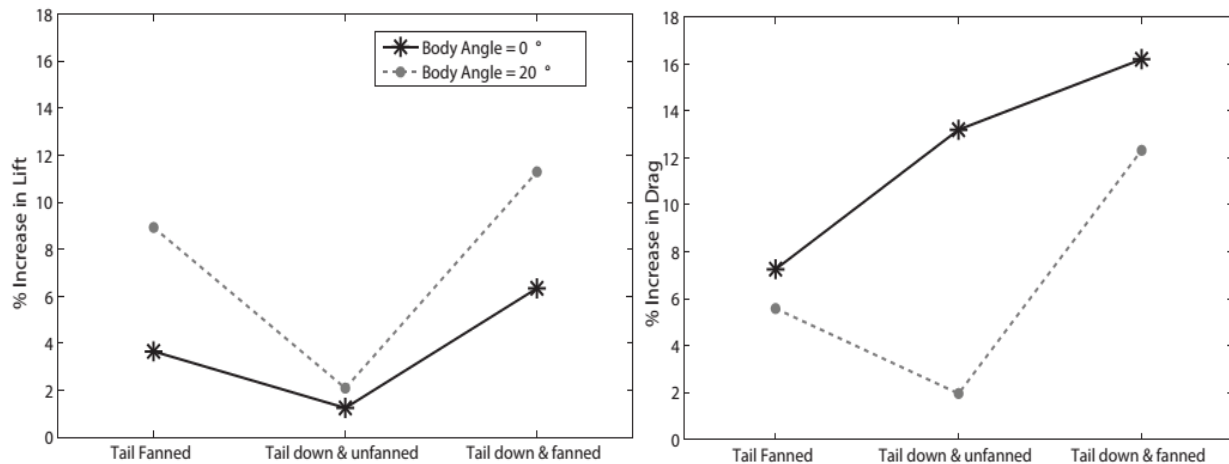


Fig. 6: Percent increase in mean (A) lift and (B) drag measured on a static hummingbird with the tail fanned and/or pitched down, relative to measurements with the tail unfanned and aligned with the body. The hummingbird body (with wings removed) was placed in different body and tail configurations in smooth airflow, and vertical (lift) and longitudinal (drag) forces were measured with a force sensor. Mean lift and drag at 0° body angle was 0.0091N and 0.0040N, respectively. Mean lift and drag at 20° body angle was 0.0156N and 0.0173N, respectively.

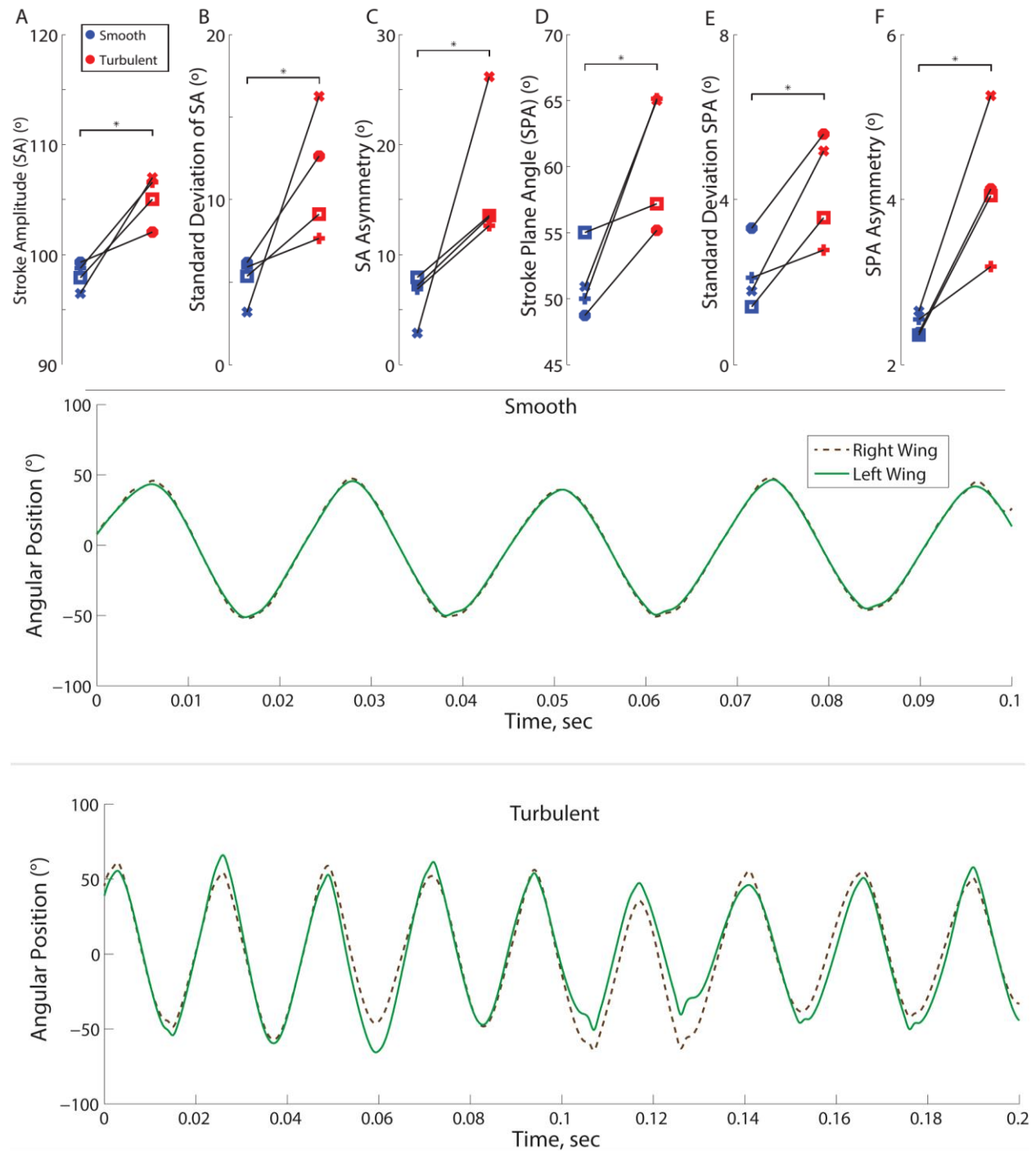


Fig. 7: Wing kinematic parameters during flight in smooth and turbulent flow. (A) Mean, (B) standard deviation, and (C) mean bilateral asymmetry of stroke amplitude in smooth (blue) and turbulent (red) flow. (D) Mean, (E), standard deviation, and (F) mean bilateral asymmetry of anatomical stroke plane angle in smooth (blue) and turbulent (red) flow. (G-H) Sample time traces of left and right wing sweep position during flight in (G) smooth and (H) turbulent flow, demonstrating increased wing asymmetry during flight in turbulence.

Supplementary Data

Table S1: Summary of turbulence properties in each flow conditions. x, y & z represent the longitudinal (downstream), lateral and vertical directions with respect to the wind tunnel.

Flow Condition	Turbulence Intensity (Ti)				Integral Length Scale (L), cm		
	Ti _x	Ti _y	Ti _z	Ti _{Tot}	Lxx	Lxy	Lxz
Smooth Flow (No Grid)	1.2%	1.1%	1%	1.2%	-	-	-
Turbulent Flow (4 x 4 cm grid)	14.33%	16.21%	15.65%	15.97%	4.12	3.6	4.64

Table S2: Standard deviations of distance maintained between the head and feeder, and absolute mean accelerations experienced by the head and body of each bird along the longitudinal, lateral and vertical directions.

Bird	Flow Condition	σ Distance between head and feeder (mm)	Head accelerations (m/s ²)			Body accelerations (m/s ²)		
			Longitudinal	Lateral	Vertical	Longitudinal	Lateral	Vertical
1	smooth	0.24	0.90	0.49	0.54	1.09	2.05	2.32
2	smooth	0.64	1.23	0.61	1.51	1.11	2.67	1.41
3	smooth	0.44	0.45	0.48	0.92	0.72	1.17	1.81
4	smooth	0.25	1.15	0.62	1.35	0.85	2.44	1.25
1	turbulent	0.21	0.69	0.64	0.99	2.04	4.61	2.86
2	turbulent	1.28	0.90	0.80	0.85	2.77	12.11	4.58
3	turbulent	1.61	1.30	0.72	0.94	1.53	4.76	3.22
4	turbulent	0.33	1.43	1.03	1.53	3.22	9.92	5.11

Table S3: Absolute mean rotation rates of the head, body and tail of each bird around the longitudinal (roll), lateral (pitch) and vertical (yaw) body axes.

Bird	Flow Condition	Head rotations (deg/s)			Body rotations (deg/s)			Tail rotations (deg/s)		
		Roll	Pitch	Yaw	Roll	Pitch	Yaw	Roll	Pitch	Yaw
1	smooth	101.43	26.31	20.94	172.37	138.53	75.95	168.18	176.03	171.16
2	smooth	211.93	39.82	40.56	208.78	95.59	105.58	238.01	218.57	188.83
3	smooth	120.26	66.49	28.79	137.24	106.26	107.33	367.61	231.96	96.286
4	smooth	181.79	63.68	23.63	153.65	104.81	42.05	100.43	87.018	67.525
1	turbulent	176.25	27.96	43.31	635.98	160.35	275.14	401.26	387.99	379
2	turbulent	123.58	65.65	50.23	711.33	246.80	208.87	449.33	356.99	687.88
3	turbulent	110.05	80.91	45.56	702.25	261.08	392.11	781.82	412.74	341.86
4	turbulent	148.94	82.28	62.02	977.01	333.95	371.59	651.24	510.98	598.69

Table S4: Mean and standard deviation of tail fan angle for each bird

Bird	Flow Condition	Mean Tail Fan Angle (deg)	σ Tail Fan Angle (deg)
1	smooth	61.11	7.71
2	smooth	57.12	7.09
3	smooth	56.82	4.22
4	smooth	65.20	1.84
1	turbulent	110.22	12.76
2	turbulent	70.89	18.27
3	turbulent	72.56	13.69
4	turbulent	88.14	12.75

Table S5: Lift and drag forces measured on a static hummingbird body with various body angles and tail configurations in smooth flow

Body AoA (deg)	Tail AoA (deg)	Tail Fan Angle (deg)	Lift, N	Drag, N
0	0	58	0.0091	0.0040
0	15	58	0.0093	0.0046
0	0	103	0.0095	0.0043
0	15	103	0.0097	0.0047
20	0	58	0.0156	0.0173
20	15	58	0.0160	0.0176
20	0	103	0.0170	0.0183
20	15	103	0.0174	0.0194

Table S6: Mean values of wing kinematic parameters for each bird

Bird	Flow Condition	Mean flapping frequency (Hz)	Mean stroke amplitude – left (deg)	Mean stroke amplitude – right (deg)	Mean stroke plane angle - left (deg)	Mean stroke plane angle – right (deg)
1	smooth	41.66	100.33	97.22	50.98	49.02
2	smooth	42.78	98.65	99.97	49.3	48.17
3	smooth	41.56	97.35	98.47	54.88	55.15
4	smooth	40.21	95.2	97.76	50.34	51.51
1	turbulent	42.78	103.72	109.45	66.81	63.47
2	turbulent	43.79	100.82	103.3	55.63	54.74
3	turbulent	43.47	107.68	102.4	56.72	57.66
4	turbulent	41.67	109.55	104.45	65.58	64.45

Table S7: Standard deviations of wing kinematic parameters for each bird

Bird	Flow	Flapping Frequency (Hz)	Stroke amplitude – left (deg)	Stroke amplitude, right, (Deg)	Bilateral asymmetry stroke amplitude, (Deg)	Max. bilateral asymmetry stroke amplitude, (Deg)	Stroke plane angle, (left) (Deg)	Stroke plane angle, (right), (Deg)	Bilateral asymmetry stroke plane angle, (Deg)	Max. bilateral asymmetry stroke plane angle, (Deg)
1	smooth	0.18	5.97	5.87	6.87	15.76	2.11	2.11	2.55	5.34
2	smooth	0.11	6.67	5.71	7.17	14.72	3.51	3.11	2.39	6.72
3	smooth	0.08	5.57	5.16	7.94	17.22	1.56	1.25	2.36	3.29
4	smooth	0.15	2.73	3.66	2.88	9.53	1.81	1.77	2.65	4.90
1	turbulent	1.1	6.70	8.61	12.64	36.19	3.05	2.51	3.19	9.00
2	turbulent	0.5	11.97	13.31	13.40	46.47	5.34	5.84	4.13	11.40
3	turbulent	0.8	8.32	9.93	13.55	38.11	3.62	3.51	4.05	8.64
4	turbulent	0.8	15.76	16.76	26.17	40.21	4.25	6.11	5.26	9.45

Fig. S8: Representative time series showing absolute roll angle of the body and tail fan angle for bird 2 in turbulent flow. Rapid increases in tail fan angle are correlated with high roll angles of the body.

